

A unifying mechanism for conductivity and magnetism at interfaces of insulating nonmagnetic oxides

Liping Yu and Alex Zunger

University of Colorado, Boulder, Colorado 80309, USA

The discovery of conducting two-dimensional electron gas (2DEG) and magnetism at the interface between insulating nonmagnetic oxides, as exemplified by the polar LaAlO₃ and nonpolar SrTiO₃ has raised prospects for attaining interfacial functionalities absent in the component materials. Yet, the physical origin of such emergent phenomena remains unclear, posing obstacles to design of improved functionalities. Using first principles defect theory we reveal a unifying mechanism for both conductivity and magnetism. We demonstrate that the polar-discontinuity-induced electric field in the LaAlO₃ film triggers thermodynamically the spontaneous formation of surface defects at some critical thickness. The electrons ionized from these surface donors are transferred by the internal electric field to the SrTiO₃, creating an interfacial 2DEG and setting up a counter field that resolves the divergence of built-up electric potential in LaAlO₃. The Al-on-Ti anti-site acceptors at the interface trap part of the 2DEG, whereas the Ti-on-Al anti-site donors lead to interface magnetism. Our results suggest practical design guidelines for inducing and controlling both 2DEG and magnetism at polar-nonpolar oxide interfaces.

Oxide interfaces exhibit many spectacular phenomena not found in the respective bulk components or in conventional semiconductor interfaces¹, providing new avenues for electronics². The LaAlO₃/SrTiO₃ interface is a paradigm example, exhibiting conducting 2DEG^{3,4} and magnetism⁵⁻¹¹ between two insulating nonmagnetic metal-oxides. In the [001] direction, two different interfaces can be formed between polar LaAlO₃, which consists of alternating LaO⁺-(AlO₂)⁻ layers, and nonpolar SrTiO₃, which consists of alternating (SrO)⁰-(TiO₂)⁰ layers. One is called n-type (i.e., LaO/TiO₂) and the other is called p-type (i.e., AlO₂/SrO). The remarkable feature is that the conductivity occurs only at n-type interfaces when the LaAlO₃ film thickness (n_{LAO}) is larger than three unit cells (uc)^{4,5}, whereas the magnetism has been observed both at n-type interfaces with $n_{LAO} > \sim 3$ uc and at insulating p-type interfaces⁸. As listed in Table 1, this feature and other experimental observations represent the main puzzles¹² that need to be resolved before the promised applications can be realized.

Four main mechanisms have been suggested to explain the 2DEG at n-type interfaces. The prevalent model is the so-called polar catastrophe scenario^{3,4}, a process in which electrons transfer from the LaAlO₃ valence bands to the SrTiO₃ conduction bands, mitigating the divergence of the built-up electrical potential as n_{LAO} increases, owing to the polar discontinuity across the interfaces. This defect-free model predicts a significant internal field in ultrathin LaAlO₃ film, contrary to the tiny field found in experiments¹³⁻¹⁶. Two of the other suggested mechanisms are based on the *interfacial donor* defects within SrTiO₃ substrate, namely, oxygen vacancies (denoted as V_O(*I*), where “*I*” means *Interface*)¹⁷⁻¹⁹ and La-on-Sr (La_{Sr}) antisite defects induced by interfacial cation intermixing²⁰⁻²⁶. These defects induced by growth, however, do not explain the appearance of a critical thickness (L_c) in the problem. The fourth mechanism is oxygen vacancies at LaAlO₃ overlayer *surface* (denoted as V_O(*S*), where *S* means *Surface*)²⁷⁻³¹. Such V_O(*S*) predicted to exist only when $n_{LAO} > \sim L_c$ cannot explain the experimentally observed weak residual field in LaAlO₃ film with $n_{LAO} < L_c$ ¹³. Hence, a unifying consensus for the leading 2DEG phenomena (Table 1) is still missing².

The origin of interface magnetism is also unclear and under debate. Experimentally⁵⁻¹¹, it is established that the magnetism is associated with Ti³⁺ ions. However, it is yet unclear whether interface magnetism resides in SrTiO₃, or LaAlO₃, or both. Theoretically, the magnetism has been postulated to arise in SrTiO₃ side, involving the occupation of the low-energy Ti-*d_{xy}*-like sub-bands caused by the interfacial

splitting of orbital degeneracy³², or interfacial disorder^{33,34}, or interfacial oxygen vacancies³⁵. However, the electrons occupying such low-energy sub-bands have light in-plane effective mass³⁶. They thus should be itinerant and lead to interface conductivity as well. Therefore, the models based on interfacial Ti^{3+} at SrTiO_3 side are difficult to reconcile why the magnetism appears at insulating p-type interfaces and at n-type interfaces with a critical thickness similar to that for 2DEG. On the other hand, the dynamical mean-field theory does not suggest a stable magnetic ground state in such scenarios³⁷.

Here using first principles theory, we studied both electronic and defect properties for both types of $\text{LaAlO}_3/\text{SrTiO}_3$ interfaces (see Methods). For defect, both formation energy (deciding its equilibrium concentration) and the transition energy levels (i.e., donor or acceptor levels, deciding if it contributes free carriers) have been calculated. We uncover a unifying mechanism (Fig.1) that identifies the origin of both conductivity and magnetism and reconciles previous mechanisms for them. **For n-type interfaces**, the 2DEG originates from $V_{\text{O}}(S)$, whereas its density is controlled by the concentration of interfacial acceptor defects (mainly Al_{Ti} antisite) that trap free electrons. The observed weak electric field in LaAlO_3 film with $n_{\text{LAO}} < L_c$, which cannot be reconciled by $V_{\text{O}}(S)$, is due to the compensation by the electron transfer from surface Ti_{Al} donor defects to interfacial Al_{Ti} acceptor defects. The interfacial point defects (La_{Sr} and V_{O}) that have been suggested to be responsible for 2DEG²⁰⁻²⁶ turn out to be not responsible. **For p-type interfaces**, the insulating nature is attributed to the defects formed at interface and surface. The charge transfer from the interfacial defects (La_{Sr}) to the surface defects (Sr_{La} or V_{La}) always eliminates the polar field (also band-bending) in LaAlO_3 film. The band edges are thus too far way from the resulting Fermi energy (E_F) that pins around the middle of SrTiO_3 band gap. Hence no free carrier can arise from the depopulation of the valence or conduction bands in both interface and surface region (whence insulating). **For both types of interfaces**, the interface magnetism originates from *un-ionized* (charge neutral) deep Ti_{Al} (i.e., Ti^{3+} -on- Al^{3+}) defects at the LaAlO_3 side near the interface, distinct from the models that are based on the Ti^{3+} at SrTiO_3 side³²⁻³⁵.

The distinctive feature of this unifying mechanism is that the built-in field in polar LaAlO_3 film is mitigated by the charge transfer from the defects at LaAlO_3 surface to the interface within nonpolar SrTiO_3 side. This feature is general for polar-nonpolar interfaces, not limited to $\text{LaAlO}_3/\text{SrTiO}_3$ case. The nonzero built-in field in the polar film of an abrupt polar-nonpolar interface reduces the formation energy (ΔH) required to form defects at the surface of the polar film (or defect pairs across the interface), as the thickness of the polar film increases. This ΔH -reduction triggers at some L_c the *spontaneous (exothermic)* formation of defects that may require high ΔH to form in the corresponding *bulk* components. The charges transfer from these spontaneously formed surface defects in turn cancels the polar field. Once the polar field is cancelled, the ΔH of those field-induced defects returns to its initial value like in the bulk. Thus, in general, the ground state of polar-nonpolar interface structure is not defect-free. The ensuing defects are then responsible for the creation and compensation of free carriers and for interface magnetism.

We next explain more specifically how this mechanism resolves the main outstanding puzzles and critical experimental observations listed in Table 1, identifying the design principles for controlling both conductivity and magnetism $\text{LaAlO}_3/\text{SrTiO}_3$ interfaces and for discovering other oxide interfaces that exhibit similar emergent phenomena.

What creates the 2DEG?

The 2DEG unlikely originates from intrinsic LaAlO_3 valence bands within the polar catastrophe model^{3,4} or from LaO -interface layer within interfacial charge leaking model³⁸. This is because that the creation of 2DEG by both models in defect-free scenario require LaAlO_3 valence band maximum (VBM) cross the SrTiO_3 conduction band minimum (CBM) or Fermi-energy E_F , contrary to the

experimentally observed weak field (or ignorable band-bending)¹³⁻¹⁶ in LaAlO₃ film that clearly suggest that LaAlO₃ VBM is far below the E_F .

The 2DEG also unlikely originates from *interfacial* point donor defects (La_{Sr}, Ti_{Al}, and V_O). Our calculated equilibrium E_F of the system always stays within the upper half of the SrTiO₃ band gap (shaded area in Fig.2a). For E_F in such range, Fig.2a shows the La_{Sr} and Ti_{Al} antisite defects have negligible or negative ΔH and can form spontaneously, causing inevitable cation intermixing. However, they do not produce itinerant carriers because they are stable at their charge neutral states. For interfacial V_{O(I)} defects, they too have high ΔH (>2.5 eV) to form in any significant amount that matters, though they are shallow donors that can contribute to 2DEG. Thus, contrary to earlier postulations, these interfacial donor defects do not contribute to 2DEG, consistent with recent experiments³⁹.

The surface V_{O(S)} defects can lead to interface 2DEG. For this to happen, three conditions need to be satisfied. First, V_{O(S)} needs to have sufficiently low ΔH so it could form. Fig.3a shows the ΔH of V_{O(S)} decreases linearly as n_{LAO} increases, consistent with previous calculations^{30,40}. When the ΔH goes through zero at $n_{LAO} \sim 3-4$ uc, the V_{O(S)} will form spontaneously. Second, the donor level of V_{O(S)} should be higher in energy than the SrTiO₃ conduction band edge at the interface. Fig.2 shows that this condition is also satisfied. Third, the system needs to have a none-zero built-in polar field that enables the charge transfer across a large distance in a direction that sets up an opposite dipole, which in turn cancels the field and lead to an energetically more stable state. Without such a field, the long-distance charge transfer is unlikely since it would create a large dipole that would increase the electrostatic energy (proportional to that dipole) and thus destabilize the system. These three conditions are satisfied in this LaAlO₃/SrTiO₃ system. The emerging picture thus is that the electrons ionized from V_{O(S)} transfer to the SrTiO₃ conduction bands at the interface via built-in polar field, forming 2DEG there. This charge transfer in turn cancels the built-in field in LaAlO₃. After the built-in field has been cancelled, the ΔH of V_{O(S)} return to a high value (> 3 eV) like that in the bulk, and V_{O(S)} are hard to form anymore in thermodynamic equilibrium³⁰. Thus, the maximum concentration of V_{O(S)} is $0.25/S_{2D}$ (where S_{2D} is 2D unit cell area), i.e., one of eight oxygen missing at surface, donating $0.5 e/S_{2D}$ that cancels the polar field in LaAlO₃ completely.

The compensation of polar field by V_{O(S)} also means that the band bending in LaAlO₃ due to polar field is also removed. Thus, the LaAlO₃ valence bands fall well below the E_F , and no free holes can arise from depopulated LaAlO₃ valence bands at the surface (whence insulating), consistent with experiments^{3,31}.

The emerging design principle for selecting materials that will likely form interface 2DEG is to find a polar material with some donor defects, similar to V_O in this case, whose properties satisfy the aforementioned three conditions. This picture suggests that the 2DEG at n-type LaAlO₃/SrTiO₃ interfaces may also be induced and/or tuned by using some surface adsorbates (e.g., H₂O, H)^{41,42} or metallic contacts⁴³ provided that the ionization energy of the surface adsorbate or the metallic contact is not lower than the SrTiO₃ conduction band edge at the interface.

What controls the critical thickness?

The linear decreasing ΔH of V_{O(S)} with increasing n_{LAO} naturally explains the critical thickness L_c for the metal-insulator transition. The decreasing rate (i.e., the slope $d\Delta H/dn_{LAO}$) equals $0.19 \text{ eV}/\text{\AA}$, which is same as the calculated built-in polar field ($E_{built-in}$) in the defect-free LaAlO₃ film (Supplementary Fig.1d). The V_{O(S)} defects start to form spontaneously when the ΔH becomes zero at an L_c of ~ 4 uc under a typical O-rich growth condition (Fig.3a). For the LaAlO₃ film that is one unit cell thinner than this L_c , the calculated ΔH of V_{O(S)} is 0.75 eV , which is too high to produce significant free carrier

concentration. Thus, the appearance of $V_O(S)$ (and the ensuing metal-insulator transition) at L_c is sharp, distinct from the gradual appearance of 2DEG behavior as predicted from polar catastrophe model (Supplementary Fig. 1e).

Fig.3a suggests that the L_c resulting from $V_O(S)$ is controlled by the formation energy ΔH_o of V_O at interface (or ΔH extrapolated at $n_{LAO} = 0$) and the $E_{built-in}$ via $L_c = \Delta H_o / eE_{built-in}$. Since $E_{built-in} = 4\pi P_0 / \epsilon$ (where ϵ and P_0 are the dielectric constant and formal polarization of LaAlO_3 film), this relation can be written as $L_c = \Delta H_o \epsilon / 4\pi e P_0$, which predicts an L_c of ~ 4 uc, depending slightly on the O-poor/rich growth conditions (Supplementary discussion). The relation of $L_c = \Delta H_o \epsilon / 4\pi e P_0$ provides an alternative explanation for the observed variation of the L_c with the fraction x in $(\text{LaAlO}_3)_{1-x}(\text{SrTiO}_3)_x$ overlayer (where P_0 is proportional to x)⁴⁴. This observation was originally explained by $L_c = \Delta \Phi \epsilon / 4\pi e P_0$ (where $\Delta \Phi$ is the energy difference between LaAlO_3 VBM and SrTiO_3 CBM) within polar catastrophe model⁴⁴. Since $\Delta \Phi$ and ΔH_o have similar value ($\sim 3-4$ eV), it is not surprising that the L_c predicted from these two models is also similar.

Implication on carrier mobility: the relatively high 2DEG mobility can be enabled by a modulated doping effect⁴⁵, whereby the source of carriers (LaAlO_3 surface) is spatially separated from the place where the carriers reside (the $\text{LaAlO}_3/\text{SrTiO}_3$ interface), thus minimizing carrier scattering by ionized defects. This minimal spatial separation is measured by the L_c . The $L_c = \Delta H_o \epsilon / 4\pi e P_0$ relationship suggests that a large L_c (hence maintaining good mobility) may be achieved by designing a polar materials with small polarization, large dielectric constant, and shallow donor defects with high formation energy ΔH (which also depends on the growth condition) in bulk or at the polar-nonpolar interface. Obviously, the low effective electron mass of the low-energy interfacial bands and the low interfacial defect concentration are also advantageous for achieving high mobility.

What compensates the built-in polar field?

Experimentally, only very weak residual field has been observed in LaAlO_3 film no matter whether its thickness is below or above the L_c ¹³⁻¹⁶. Neither the polar catastrophe model (Supplementary Fig. 1b), nor the interfacial point defects model, can explain this observation. The $V_O(S)$ model explains the weak electric field in LaAlO_3 film *above* the L_c , but not below the L_c . To explain the weak electric field in LaAlO_3 film *below* the L_c , we examined the role of the cation defects across the interface.

For $n_{LAO} < L_c$, the spontaneous formation of antisite defect pair $[\text{Al}_{\text{Ti}} + \text{Ti}_{\text{Al}}]$ via a $\text{Ti} \leftrightarrow \text{Al}$ exchange is responsible for the compensation the electric field in LaAlO_3 film. Previous first-principles calculation⁴⁶ found that the energy required to form such defect pair is negative (i.e., exothermic), and the largest energy gain is obtained when a Ti atom of TiO_2 -interface layer is exchanged with an Al of AlO_2 -surface layer, i.e., $\text{Al}_{\text{Ti}}(I) + \text{Ti}_{\text{Al}}(S)$ ⁴⁶. Our calculation for $n_{LAO} = 4$ uc (filled symbols in Fig.3b) shows the same feature, meaning that Ti atom at the interface would hop to the AlO_2 surface layer and exchange with Al atom there. Since the Ti_{Al} donor level is higher in energy than the Al_{Ti} acceptor defect (Fig.1a and Fig.2a), the electrons ionized from $\text{Ti}_{\text{Al}}(S)$ donor will transfer to the $\text{Al}_{\text{Ti}}(I)$ acceptor, setting up opposite dipole that largely cancels the electric field in LaAlO_3 film below the L_c . This charge-transfer between the deep defects induces no itinerant carriers, consistent with the insulating behavior observed below the L_c . Once the polar field in LaAlO_3 has been completely cancelled (e.g., by surface V_O , open symbols in Fig.3b), the ΔH of such pairs becomes positive and larger than ~ 0.4 eV, which is too high for them to form further under normal growth temperatures. It means that the maximum concentration of $[\text{Al}_{\text{Ti}} + \text{Ti}_{\text{Al}}]$ defect pairs is around $0.5/S_{2D}$, which corresponds to the complete cancellation of the field in LaAlO_3 film.

For $n_{LAO} \geq L_c$, the electric field in LaAlO_3 is compensated by $V_O(S)$ instead of $[\text{Al}_{\text{Ti}}(S) + \text{Ti}_{\text{Al}}(I)]$. This is because that V_O has a higher donor level than Ti_{Al} (Fig.1b and Fig.2a), the charge transfer from $V_O(S)$ to

$\text{Al}_{\text{Ti}}(I)$ is energetically more stable than that from Ti_{Al} to $\text{Al}_{\text{Ti}}(I)$, if both $V_{\text{O}}(S)$ and $[\text{Al}_{\text{Ti}}(S)+\text{Ti}_{\text{Al}}(I)]$ form. Indeed, if the electric field has been cancelled by $V_{\text{O}}(S)$, the $[\text{Al}_{\text{Ti}}+\text{Ti}_{\text{Al}}]$ pairs cannot form further. It can be easily understood from Fig.3b showing that the ΔH of $[\text{Al}_{\text{Ti}}+\text{Ti}_{\text{Al}}]$ pair changes from negative to positive (0.4-0.7 eV) and become almost invariant with respect to the distance between the defect-pair components. It is worth noting that the $[\text{Al}_{\text{Ti}}(S)+\text{Ti}_{\text{Al}}(I)]$ pairs formed below the L_c can not prevent $V_{\text{O}}(S)$ formation. This is because that such pairs formed in the LaAlO_3 with a given n_{LAO} do not cancel the electric field in the additional unit cell of LaAlO_3 that is going to be grown on top of it during the layer-by-layer epitaxial growth. The field in additional unit cell of LaAlO_3 induce the formation of $V_{\text{O}}(S)$ when $n_{\text{LAO}} \geq L_c$.

What controls the density of 2DEG?

According to Gauss's law, the experimentally observed weak electric field in LaAlO_3 film means that the total net charge density at the interface must be $\sim 0.5 e/S_{2D}$. For $n_{\text{LAO}} < L_c$, the insulating character means that all interfacial charge does not contribute to conductivity. For $n_{\text{LAO}} \geq L_c$, the measured 2DEG density significantly smaller than $0.5 e/S_{2D}$ means that most of the interfacial charge does not contribute to conductivity either. The real puzzle thus actually is why the majority of $0.5 e/S_{2D}$ charge that indeed exists at the interface does not contribute to conducting 2DEG. This puzzle cannot be explained within defect-free interface scenario by polar catastrophe model^{3,4} or interfacial charge leaking model⁴⁶, since both models predict (i) zero interfacial net charge for $n_{\text{LAO}} < L_c$ and (ii) an interfacial charge density much higher than the measured 2DEG density and smaller than $0.5 e/S_{2D}$ for $n_{\text{LAO}} \geq L_c$ (Supplementary Fig.1e). The possibility of multiple carrier types (i.e., electrons occupying different subbands (d_{xy} , d_{xz}/d_{yz}) contribute differently in transport) at ideal interfaces has also been suggested^{36,47-49}. However, they are difficult to reconcile why a full carrier density of $0.5 e/S_{2D}$ has been observed at $\text{GdTiO}_3/\text{SrTiO}_3$ interfaces (where the same multiple carrier types exist)⁵⁰.

We find here that the density of 2DEG is controlled by the concentration of interfacial acceptor defects that trap electrons. For any n_{LAO} , the interfacial net charge is always $\sim 0.5 e/S_{2D}$, which corresponds to the (almost) complete cancellation of the polar field in LaAlO_3 film. For $n_{\text{LAO}} < L_c$, all interfacial charge transferred from $\text{Ti}_{\text{Al}}(S)$ defects is trapped by $\text{Al}_{\text{Ti}}(I)$ acceptor defects and thus no 2DEG can occur. For $n_{\text{LAO}} \geq L_c$, the major part of $0.5 e/S_{2D}$ charge transferred from $V_{\text{O}}(S)$ is also trapped by $\text{Al}_{\text{Ti}}(I)$ defects. Fig.2a shows that the antisite defect has much lower ΔH than cation vacancy within the same interface layer at allowable E_F (shaded area). It means that the La_{Sr} and Al_{Ti} are the dominant defects in SrO and TiO_2 interface layer respectively. Since La_{Sr} is a donor that does not trap electrons and other acceptor defects (V_{Sr} and V_{Ti}) have marginal concentration, the Al_{Ti} defects are the most potent source of electron trapping. Such trapping, in general, is not complete. It is because that the complete trapping would lower the E_F back to a level similar to the E_F below the L_c , i.e., slightly above the middle of SrTiO_3 band gap. At such E_F , the Al_{Ti} defects have too high ΔH to form in term of point defects. The $[\text{Al}_{\text{Ti}}+\text{Ti}_{\text{Al}}]$ defect pair induced by $\text{Al} \leftrightarrow \text{Ti}$ exchange in the zero field has a ΔH of 0.4-0.7 eV (open symbols in Fig.3b), which is also too high for the resulting Al_{Ti} defects to form in a quantity that can trap all $0.5e/S_{2D}$ charge transferred from $V_{\text{O}}(S)$. Therefore, it is expected that only a fraction of $0.5 e/S_{2D}$ can cause conducting 2DEG when $n_{\text{LAO}} \geq L_c$.

From above, the recently observed LaAlO_3 cation-stoichiometry effect on 2DEG formation³⁹ may also be understood. For Al-rich LaAlO_3 film, where both A-site and B-site sublattices are fully occupied (hence having no cation vacancies), the Al_{Ti} anti-sites are the only electron-trapping defects and the incomplete trapping of $0.5e/S_{2D}$ interface charge by Al_{Ti} defects leads to interface conductivity. However, for La-rich LaAlO_3 film, where B-site sublattice is not fully occupied, the cation vacancies (V_{Ti} and V_{Al}) also become main electron-trappers, in addition to $\text{Al}_{\text{Ti}}(I)$. Though, the concentration of Al_{Ti} is reduced, each cation vacancy induced in La-rich film traps more electrons than an Al_{Ti} . The

insulating character can be then attributed to the complete interfacial electron trapping by both interfacial cation vacancies and $Al_{Ti}(I)$.

The picture of $Al_{Ti}(I)$ as main electron-trapping defects may be extended to $SrTiO_3/GdTiO_3$ interfaces. The observed full carrier density of $0.5 e/S_{2D}$ there⁵⁰ can be ascribed to the fact that both $SrTiO_3$ and $GdTiO_3$ have the same Ti atom at B-site sublattice and have no Al_{Ti} -like antisite defects at the interface.

Implication on how to enhance 2DEG: The above picture suggests that the main controlling factor for the interface carrier density is the concentration of the acceptor defects (mainly Al_{Ti} in stoichiometric or Al-rich film), which should be minimized for enhancing carrier density. Such Al_{Ti} -like electron trapping defects may be completely removed by designing other oxide interfaces like $GdTiO_3/SrTiO_3$ interfaces, whose bulk components have a common cation atom with multiple valence states.

Why are the p-type interfaces insulating?

An intriguing fact is that the p-type interface is insulating and not p-type. The polar-catastrophe model for p-type interface structures predicts hole conducting interface and electron conducting surface when $n_{LAO} > \sim 7.3$ uc (Supplementary Fig.1) in contradiction with experiment. To explain the experimentally observed insulating behavior there, the defects thus must be involved. The emerging defect picture below differs from the model based solely on interfacial hole-polaron⁵¹ or interfacial hole-compensating V_O defects^{20,40}, which assumes that the interface has holes arising from the depopulation of $SrTiO_3$ valence bands.

Generally, for polar-nonpolar interface structure, the linear decreasing ΔH of certain surface defect with increasing polar-film thickness is a sign of polar-field compensation by the charge transfer from/or the surface defect. For n-type $LaAlO_3/SrTiO_3$ interfaces, this is the case for $[Ti_{Al}(S)+Al_{Ti}(I)]$ when $n_{LAO} < L_c$ (Fig.3b) and $V_O(S)$ when $n_{LAO} \geq L_c$ (Fig.3a). For p-type $LaAlO_3/SrTiO_3$ interfaces, similarly, the polar field is compensated by the charge transfer among the spontaneously formed $[La_{Sr}(I)+Sr_{La}(S)]$ defect pairs when $n_{LAO} < \sim 4$ uc (Fig.3d). When $n_{LAO} \geq \sim 4$ uc, the polar field is compensated by the spontaneously formed $[La_{Sr}(I)+V_{La}(S)]$ defect complex (Fig.3c). Such polar-field compensation feature is expected since the acceptor levels of both Sr_{La} and V_{La} defects are lower than the donor level of La_{Sr} defect (Fig.2b). For $n_{LAO} \geq \sim 4$ uc, it is also expected that the electrons prefer to be transferred to the V_{La} defects rather than to Sr_{La} defects, since V_{La} acceptor level is lower than Sr_{La} acceptor level (Fig.2b).

The compensation of the polar field by the charge transfer among the defects suggests that there is no band bending in the $LaAlO_3$ film of any thickness (Fig.1c,d). The calculated equilibrium E_F according to those point defects turns out to stay always around the middle of $SrTiO_3$ band gap (shaded area in Fig.2b). It means that both VBM and CBM are far away from the E_F and there are no free carrier arising from the depopulation of VBM and CBM in both interface and surface regions (whence insulating).

Similar to that in Fig.2a for n-type interfaces, Fig.2b also shows that the interfacial La_{Sr} and Ti_{Ar} are deep defects with negligible or even negative ΔH at equilibrium E_F , causing inevitable interfacial cation intermixing but inducing no free carriers. The interfacial V_O defects have too high ΔH to form in sufficient quantities that can be responsible for hole-compensation as suggested previously^{20,40}.

What causes interface magnetism?

Distinct from previous models³²⁻³⁵ that are based on interfacial Ti^{3+} within $SrTiO_3$ side, we find below that the local magnetic moment originates from the un-ionized deep Ti_{Al} (i.e., Ti^{3+} -on- Al^{3+}) antisite

defects within LaAlO_3 side near the interface. The interface magnetism depends on the concentration and spatial distribution of such Ti_{Al} defects. This picture explains not only why the magnetism appears at n-type interfaces with a similar critical thickness to that for 2DEG, but also why the magnetism also appears at insulating p-type interfaces⁸.

For n-type interfaces, when $n_{\text{LAO}} < L_c$, the polar field in LaAlO_3 is cancelled by the charge transfer from $\text{Ti}_{\text{Al}}(\text{S})$ defects to the interface. These formed Ti_{Al} defects are thus ionized, i.e., $\text{Ti}^{4+}\text{-on-Al}^{3+}$, having no local magnetic moment. When $n_{\text{LAO}} \geq L_c$, the polar field in LaAlO_3 is cancelled by the charge transfer to the interface from $\text{V}_{\text{O}}(\text{S})$ instead of Ti_{Al} . All $\text{Ti}_{\text{Al}}(\text{I})$ defects in LaAlO_3 film of zero internal field are most stable in their charge neutral states (i.e., not ionized) (Fig.2b), i.e., $\text{Ti}^{3+}\text{-on-Al}^{3+}$, having a local magnetic moment. Therefore, the interface magnetism at n-type interfaces due to those un-ionized Ti_{Al} defects should also have a critical thickness of $\sim 4\text{uc}$. For p-type interfaces, it is the charge transfer among the defects other than Ti_{Al} defects that cancels the polar field in LaAlO_3 . So all formed Ti_{Al} defects there are not ionized, having local magnetic moments, and can cause interface magnetism.

The local moment of a single Ti_{Al} defect at the interface may be estimated from that in bulk LaAlO_3 , which is $0.84\mu_B$ from our hybrid functional calculation. For ferromagnetic order as observed in experiment, the total interface magnetic moment depends on the concentration of un-ionized Ti_{Al} defects in LaAlO_3 and can be very small per Ti atom in average. The experimentally observed inhomogeneous landscape of magnetism that also varies from sample to sample^{8,9} may be attributed to the various spatial distributions of Ti_{Al} defects, which may be sensitive to sample preparation conditions (such as temperature and P_{O_2}) and local strain.

Relative to $\text{V}_{\text{O}}(\text{I})$, the Ti_{Al} as the origin of magnetism is more favorable in at least two aspects. First, the deep Ti_{Al} defect is spatially localized and has an unambiguous local moment. While for V_{O} , which is a shallow donor, it donates electrons to the lower-energy interfacial Ti d_{xy} sub-bands that are delocalized inside the interface plane, and the resulting Ti^{3+} may then be itinerant. Second, the Ti_{Al} defects would form easily or even inevitable due to its small or negative ΔH , whereas the interfacial V_{O} require significant energy to form and if formed they may be removed completely after annealing.

Discussion

The emerging unifying mechanism for both conductivity and magnetism not only simultaneously reconciles the experimental observations listed in Table 1, but also predicts following distinct features that may be tested in experiment as further validation: (i) For n-type interfaces, the AlO_2 -surface layer is dominated by Ti_{Al} defects when $n_{\text{LAO}} < L_c$ and by V_{O} defect when $n_{\text{LAO}} \geq L_c$. (ii) For p-type interfaces, the LaO -surface layer is dominated by Sr_{La} and V_{La} defects, respectively, below and above an L_c of ~ 4 uc. (iii) Ti^{4+} and Ti^{3+} signals exist in both sides of the interface. The appearance of the Ti^{3+} signals should not be taken as a sign of conductivity. Whether the Ti^{3+} signals detected by photoemission below the L_c ^{15,52} can be truly assigned to those Ti^{3+} ions in SrTiO_3 side should be revisited carefully. How these Ti_{Al} local moments are ordered (ferromagnetic, or antiferromagnetic, or else) and whether/how they interact with the itinerant 2DEG are still open questions that should be investigated further.

Methods

All calculations were performed using DFT and plane-wave projector augmented-wave (PAW)⁵³ method as implemented in the VASP code⁵⁴. An energy cutoff of 400 eV was used. The Brillouin zone was sampled by $8 \times 8 \times 1$ and $4 \times 4 \times 1$ k-point mesh for 1×1 and 2×2 in-plane supercell respectively. The atomic forces were relaxed to be less than 0.03 eV/Å. The in-plane lattice constant was fixed to 3.943 Å (the GGA relaxed lattice constant of SrTiO₃). In slab calculations, the 4 uc (~16 Å) vacuum layer was used and the dipole correction was always applied to remove artificial dipole interactions⁵⁵. The results in Fig.2 were obtained by using HSE hybrid functional on the top of the GGA relaxed structures.

The formation energy of a defect (D) calculated from $\Delta H_D^q(E_F, \mu) = E_D^q - E_H + \sum_{\alpha} n_{\alpha} (\mu_{\alpha}^0 + \Delta\mu_{\alpha}) + q(E_v + E_F)$, where E_D^q and E_H are the total energies of a supercell with and without defect, respectively, and D being in charge state q . n_{α} is the number of atoms of specie α needed to create a defect. E_F is the Fermi energy relative to VBM (E_v). $\Delta\mu_{\alpha}$ is the relative chemical potential of specie α with respect to its elemental solid (gas) (μ^0). The equilibrium Fermi-energy was calculated self-consistently according to charge neutrality condition⁵⁶. The chemical potentials relative to their elemental solid (or gas) phase are taken as variables and are bounded by the values that maintain a stable host compound and avoid formation of other competing phases in thermodynamic equilibrium (Supplementary Fig.2). The details of theory and calculations can be found in Ref.[⁵⁷].

Acknowledgements

This work was supported by the US Department of Energy, Office of Basic Energy Sciences as part of an Energy Frontier Research Centers, under the award No. DE-AC36-08GO28308 to National Renewable Energy Laboratory (NREL). The computation was done by using capabilities of the NREL Computational Sciences Center supported by the U.S. DOE office of Energy Efficiency and Renewable Energy, under Contract No. DE-AC36-08GO28308.

Author Contributions

L.Y. carried out the calculations, analyzed the results and wrote the paper. A.Z. initiated this study and contributed to the analysis of the results and the writing of the paper.

Table 1: List of the main puzzles and robust experimental observations at LaAlO₃/SrTiO₃ interfaces.

Interface structure	Experimental Observations	Polar Catastrophe	Cation Mixing	V _o at interface	V _o at surface	Unifying mechanism
n-type	1. Critical thickness (L_c) = 4 uc	✓	✗	✗	?	✓
	2. 2DEG density < 0.5 e/S	✗	?	✗	✗	✓
	3. Weak E in LaAlO ₃ for $n_{LAO} < L_c$	✗	?	✗	✗	✓
	4. Weak E in LaAlO ₃ for $n_{LAO} \geq L_c$	✗	✗	✗	✓	✓
	5. LaAlO ₃ surface: insulating	✗	?	?	✓	✓
	6. Interface: cation intermixed	✗	✓	✗	✗	✓
	7. Interface magnetism	✗	?	✗	✗	✓
p-type	1. Interface: insulating	✗	?	✗	?	✓
	2. LaAlO ₃ surface: insulating	✗	✗	?	?	✓
	3. Interface: cation mixed	✗	✓	✗	✗	✓
	4. Interface magnetism	✗	?	?	✗	✓

The symbol of ‘✓’ and ‘✗’ mean that the mechanism agrees or disagrees, respectively with the experimental observation. The ‘?’ symbol denotes uncertainty.

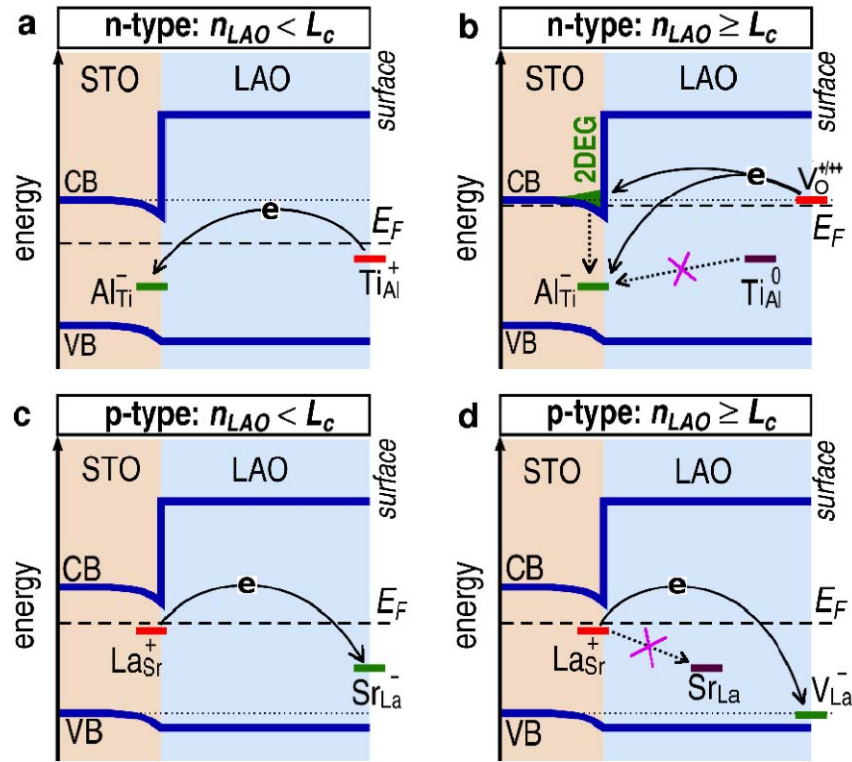


Figure 1: Schematic band and defect level picture for the unifying mechanism. **a**, n-type interfaces with $n_{LAO} < L_c$: The electrons transfer from $Ti_{Al}(S)$ to $Al_{Ti}(I)$ and compensates the electric field in $LaAlO_3$, inducing no itinerant carriers to the interface. **b**, n-type interfaces with $n_{LAO} \geq L_c$: The electrons transfer from $V_O(S)$ to interface. Part of interface charge is trapped by the deep Al_{Ti} acceptor defects. The deep Ti_{Al}^0 donor defects are confined within $LaAlO_3$ near the interface and are not ionized, i.e., Ti^{3+} -on- Al^{3+} , having local magnetic moments. **c**, p-type interfaces with $n_{LAO} < L_c$ ($\sim 4uc$): The electrons transfer from $La_{Sr}(I)$ to $Sr_{La}(S)$ and compensates the electric field in $LaAlO_3$. **d**, p-type interfaces with $n_{LAO} \geq L_c$: The electrons transfer from $La_{Sr}(I)$ to $V_{La}(S)$ and compensates the field in $LaAlO_3$. The superscripts (0,+,+,-) denote the defect charge states, not the oxidation states of the ions there.

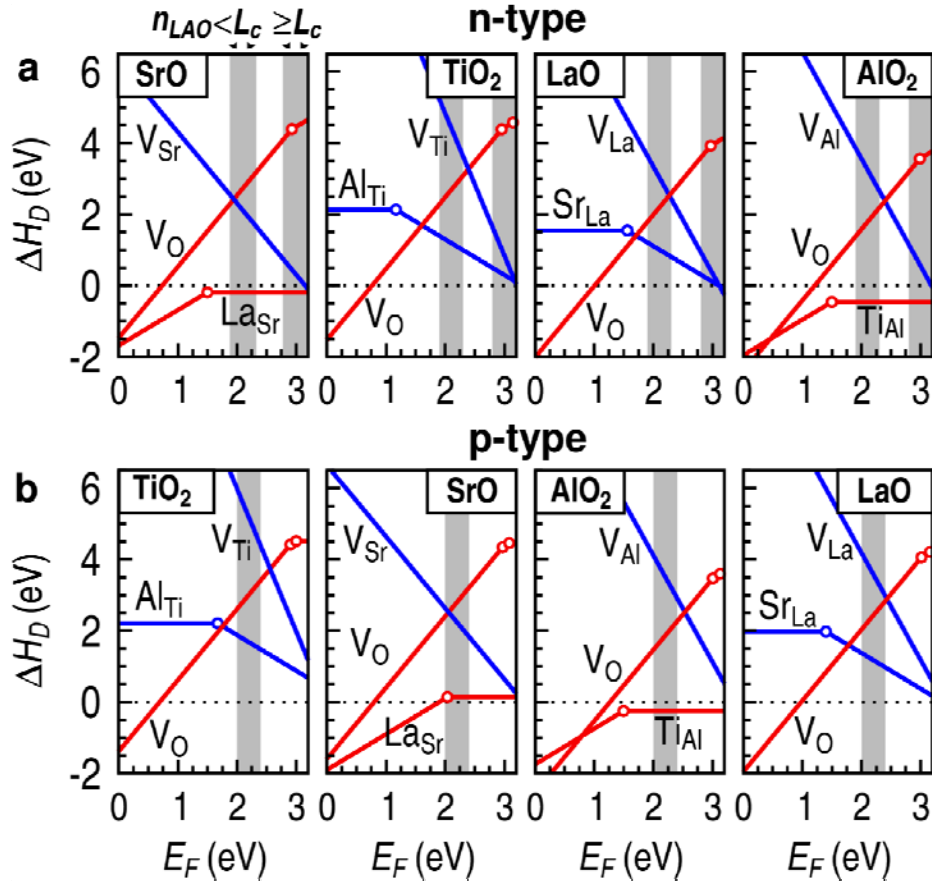


Figure 2: Properties of the interfacial point defects in the 6STO/2LAO heterostructure. a,b, the formation energy ΔH of the interfacial defects at the n-type and p-type interface, respectively, as a function of Fermi energy E_F . Each panel shows various defects in a given atomic layer. Each line represents the ΔH of a donor (red) or acceptor (blue) defect. Different slopes of line segments represent different charge states of a defect that are most stable at given E_F . Open circles mark the defect charge transition energies, i.e., donor or acceptor level defined as the E_F where the ΔH of a defect in two different charge states equal. The shaded regions in each panel denote the variation range of the equilibrium E_F , resulting from interfacial point defects only. Other cation defects that have higher ΔH are shown in Supplementary Fig. 3. The chemical potentials used for Sr, Ti, La, Al, and O are -4.36, -6.20, -6.10, -5.46, and -2.0 eV respectively, relative to their corresponding elemental solid or gas phases, which corresponds to $T=1050$ K and $P_{O_2} = 6.1 \times 10^{-6}$ Torr. To a large extent, the ΔH vs. E_F for a given defect at the same type of interfaces with different $LaAlO_3$ thickness is similar since the defect has the same local bonding and electrostatic environments at the interface.

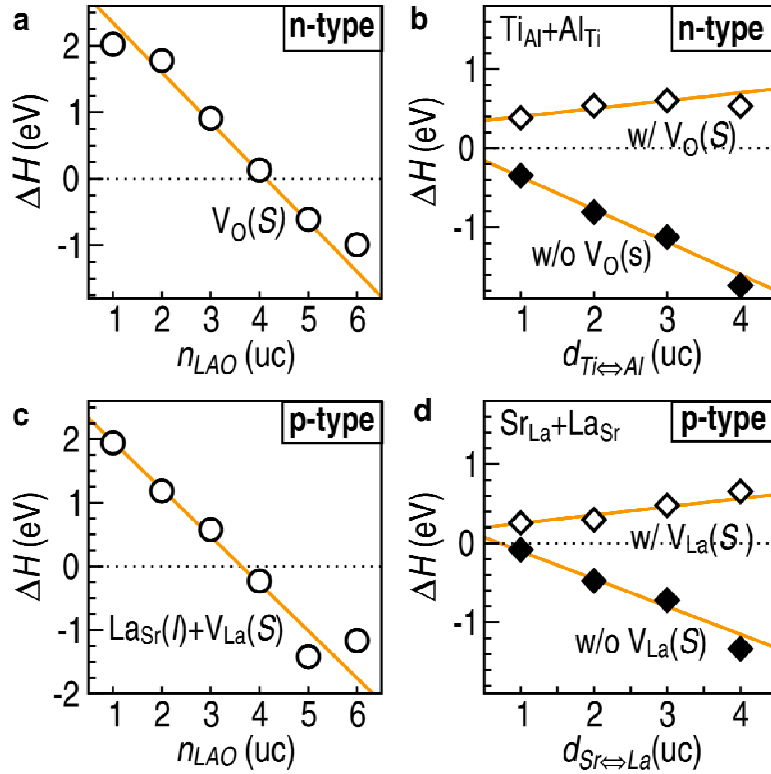


Figure 3: Properties of surface defects and defect complexes. **a**, the GGA-calculated ΔH of $V_O(S)$ defect, under the O-rich growth condition (i.e., $\Delta\mu_O = -1.5$ eV, Supplementary Fig. 2a). **b**, the ΔH of $[Ti_{Al}+Al_{Ti}]$ defect pair created from a $Ti \leftrightarrow Al$ exchange out of the ideal interface with and without a $V_O(S)$ in a 2×2 6STO/4LAO/vacuum supercell. **c**, the GGA-calculated ΔH of $[La_{Sr}(I)+V_{La}(S)]$ defect complex as a function of n_{LAO} , under $\Delta\mu_{Sr} = -4.36$ eV (Supplementary Fig. 1b). **d**, the ΔH of $[La_{Sr}+Sr_{La}]$ defect pair created from a $La \leftrightarrow Sr$ exchange out of the ideal interface with and without a $V_{La}(S)$ in a 2×2 6STO/4LAO/vacuum supercell, respectively. The $d_{Ti \leftrightarrow Al}$ and $d_{La \leftrightarrow Sr}$ in **b,d** are the distance between the components of corresponding defect pair. The orange lines are the guides to the eye.

References

- 1 Hwang, H. Y. *et al.* Emergent phenomena at oxide interfaces. *Nat Mater* **11**, 103-113 (2012).
- 2 Mannhart, J. & Schlom, D. G. Oxide Interfaces-An Opportunity for Electronics. *Science* **327**, 1607-1611 (2010).
- 3 Ohtomo, A. & Hwang, H. Y. A high-mobility electron gas at the LaAlO₃/SrTiO₃ heterointerface. *Nature* **427**, 423-426 (2004).
- 4 Thiel, S., Hammerl, G., Schmehl, A., Schneider, C. W. & Mannhart, J. Tunable quasi-two-dimensional electron gases in oxide heterostructures. *Science* **313**, 1942-1945 (2006).
- 5 Brinkman, A. *et al.* Magnetic effects at the interface between non-magnetic oxides. *Nat Mater* **6**, 493-496 (2007).
- 6 Li, L., Richter, C., Mannhart, J. & Ashoori, R. C. Coexistence of magnetic order and two-dimensional superconductivity at LaAlO₃/SrTiO₃ interfaces. *Nat Phys* **7**, 762-766 (2011).
- 7 Ariando *et al.* Electronic phase separation at the LaAlO₃/SrTiO₃ interface. *Nat Commun* **2**, 188 (2011).
- 8 Kalisky, B. *et al.* Critical thickness for ferromagnetism in LaAlO₃/SrTiO₃ heterostructures. *Nat Commun* **3**, 922 (2012).
- 9 Salman, Z. *et al.* Nature of Weak Magnetism in SrTiO₃/LaAlO₃ Multilayers. *Phys Rev Lett* **109**, 257207 (2012).
- 10 Lee, J. S. *et al.* Titanium d(xy) ferromagnetism at the LaAlO₃/SrTiO₃ interface. *Nat Mater* **12**, 703-706 (2013).
- 11 Joshua, A., Ruhman, J., Pecker, S., Altman, E. & Ilani, S. Gate-tunable polarized phase of two-dimensional electrons at the LaAlO₃/SrTiO₃ interface. *P Natl Acad Sci USA* **110**, 9633-9638 (2013).
- 12 Chen, H. H., Kolpak, A. M. & Ismail-Beigi, S. Electronic and Magnetic Properties of SrTiO₃/LaAlO₃ Interfaces from First Principles. *Adv Mater* **22**, 2881-2899 (2010).
- 13 Segal, Y., Ngai, J. H., Reiner, J. W., Walker, F. J. & Ahn, C. H. X-ray photoemission studies of the metal-insulator transition in LaAlO₃/SrTiO₃ structures grown by molecular beam epitaxy. *Phys Rev B* **80**, 241107 (2009).
- 14 Huang, B. C. *et al.* Mapping Band Alignment across Complex Oxide Heterointerfaces. *Phys Rev Lett* **109**, 246807 (2012).
- 15 Slooten, E. *et al.* Hard x-ray photoemission and density functional theory study of the internal electric field in SrTiO₃/LaAlO₃ oxide heterostructures. *Phys Rev B* **87**, 085128 (2013).
- 16 Berner, G. *et al.* Band alignment in LaAlO₃/SrTiO₃ oxide heterostructures inferred from hard x-ray photoelectron spectroscopy. *Phys Rev B* **88**, 115111 (2013).
- 17 Siemons, W. *et al.* Origin of charge density at LaAlO₃ on SrTiO₃ heterointerfaces: Possibility of intrinsic doping. *Phys Rev Lett* **98**, 196802 (2007).
- 18 Kalabukhov, A. *et al.* Effect of oxygen vacancies in the SrTiO₃ substrate on the electrical properties of the LaAlO₃/SrTiO₃ interface. *Phys Rev B* **75**, 121404 (2007).
- 19 Herranz, G. *et al.* High mobility in LaAlO₃/SrTiO₃ heterostructures: Origin, dimensionality, and perspectives. *Phys Rev Lett* **98**, 216803 (2007).
- 20 Nakagawa, N., Hwang, H. Y. & Muller, D. A. Why some interfaces cannot be sharp. *Nat Mater* **5**, 204-209 (2006).
- 21 Willmott, P. R. *et al.* Structural basis for the conducting interface between LaAlO₃ and SrTiO₃. *Phys Rev Lett* **99**, 155502 (2007).

- 22 Kalabukhov, A. S. *et al.* Cationic Disorder and Phase Segregation in LaAlO₃/SrTiO₃ Heterointerfaces Evidenced by Medium-Energy Ion Spectroscopy. *Phys Rev Lett* **103**,146101 (2009).
- 23 Yamamoto, R. *et al.* Structural Comparison of n-Type and p-Type LaAlO₃/SrTiO₃ Interfaces. *Phys Rev Lett* **107**, 036104 (2011).
- 24 Qiao, L., Droubay, T. C., Kaspar, T. C., Sushko, P. V. & Chambers, S. A. Cation mixing, band offsets and electric fields at LaAlO₃/SrTiO₃(001) heterojunctions with variable La:Al atom ratio. *Surf Sci* **605**, 1381-1387 (2011).
- 25 Vonk, V. *et al.* Polar-discontinuity-retaining A-site intermixing and vacancies at SrTiO₃/LaAlO₃ interfaces. *Phys Rev B* **85**, 045401 (2012).
- 26 Gunkel, F. *et al.* Influence of charge compensation mechanisms on the sheet electron density at conducting LaAlO₃/SrTiO₃-interfaces. *Appl Phys Lett* **100**, 052103 (2012).
- 27 Cen, C. *et al.* Nanoscale control of an interfacial metal-insulator transition at room temperature. *Nat Mater* **7**, 298-302 (2008).
- 28 Zhong, Z. C., Xu, P. X. & Kelly, P. J. Polarity-induced oxygen vacancies at LaAlO₃/SrTiO₃ interfaces. *Phys Rev B* **82**, 165127 (2010).
- 29 Bristowe, N. C., Littlewood, P. B. & Artacho, E. Surface defects and conduction in polar oxide heterostructures. *Phys Rev B* **83**, 205405 (2011).
- 30 Li, Y., Phattalung, S. N., Limpijumnong, S., Kim, J. & Yu, J. Formation of oxygen vacancies and charge carriers induced in the n-type interface of a LaAlO₃ overlayer on SrTiO₃(001). *Phys Rev B* **84**, 245307 (2011).
- 31 Berner, G. *et al.* Direct k-Space Mapping of the Electronic Structure in an Oxide-Oxide Interface. *Phys Rev Lett* **110**, 247601 (2013).
- 32 Banerjee, S., Erten, O. & Randeria, M. Ferromagnetic exchange, spin-orbit coupling and spiral magnetism at the LaAlO₃/SrTiO₃ interface. *Nat Phys* **9**, 625-629 (2013).
- 33 Fidkowski, L., Jiang, H. C., Lutchyn, R. M. & Nayak, C. Magnetic and superconducting ordering in one-dimensional nanostructures at the LaAlO₃/SrTiO₃ interface. *Phys Rev B* **87**, 014436 (2013).
- 34 Michaeli, K., Potter, A. C. & Lee, P. A. Superconducting and Ferromagnetic Phases in SrTiO₃/LaAlO₃ Oxide Interface Structures: Possibility of Finite Momentum Pairing. *Phys Rev Lett* **108**, 117003 (2012).
- 35 Pavlenko, N., Kopp, T., Tsymbal, E. Y., Mannhart, J. & Sawatzky, G. A. Oxygen vacancies at titanate interfaces: Two-dimensional magnetism and orbital reconstruction. *Phys Rev B* **86**, 064431 (2012).
- 36 Delugas, P. *et al.* Spontaneous 2-Dimensional Carrier Confinement at the n-Type SrTiO₃/LaAlO₃ Interface. *Phys Rev Lett* **106**, 166807 (2011).
- 37 Chan, C. K., Werner, P. & Millis, A. J. Magnetism and orbital ordering in an interacting three-band model: A dynamical mean-field study. *Phys Rev B* **80**, 235114 (2009).
- 38 Janotti, A., Bjaalie, L., Gordon, L. & Van de Walle, C. G. Controlling the density of the two-dimensional electron gas at the SrTiO₃/LaAlO₃ interface. *Phys Rev B* **86**, 241108 (2012).
- 39 Warusawithana, M. P. R., C.; Mundy, J. A.; Roy, P.; Ludwig, J.; Paetel, S.; Heeg, T.; Pawlicki, A. A.; Kourkoutis, L. F.; Zheng, M.; Lee, M.; Mulcahy, B.; Zander, W.; Zhu, Y.; Schubert, J.; Eckstein, J. N.; Muller, D. A.; Hellberg, C. S.; Mannhart, J.; Schlom, D. G. LaAlO₃ stoichiometry is key to electron liquid formation at LaAlO₃/SrTiO₃ interfaces. *Nat Commun* **4**, 2351(2013).
- 40 Zhang, L. X. *et al.* Origin of insulating behavior of the p-type LaAlO₃/SrTiO₃ interface: Polarization-induced asymmetric distribution of oxygen vacancies. *Phys Rev B* **82**,125412 (2010).

- 41 Xie, Y. W., Hikita, Y., Bell, C. & Hwang, H. Y. Control of electronic conduction at an oxide
heterointerface using surface polar adsorbates. *Nat Commun* **2**, 494 (2011).
- 42 Bi, F. *et al.* "Water-cycle" mechanism for writing and erasing nanostructures at the
LaAlO₃/SrTiO₃ interface. *Appl Phys Lett* **97**, 173110 (2010).
- 43 Arras, R., Ruiz, V. G., Pickett, W. E. & Pentcheva, R. Tuning the two-dimensional electron
gas at the LaAlO₃/SrTiO₃(001) interface by metallic contacts. *Phys Rev B* **85**, 125404
(2012).
- 44 Reinle-Schmitt, M. L. *et al.* Tunable conductivity threshold at polar oxide interfaces. *Nat
Commun* **3**, 932 (2012).
- 45 Dingle, R., Stormer, H. L., Gossard, A. C. & Wiegmann, W. Electron Mobilities in Modulation-
Doped Semiconductor Heterojunction Super-Lattices. *Appl Phys Lett* **33**, 665-667 (1978).
- 46 Chambers, S. A. *et al.* Instability, intermixing and electronic structure at the epitaxial
LaAlO₃/SrTiO₃(001) heterojunction. *Surf Sci Rep* **65**, 317-352 (2010).
- 47 Popovic, Z. S., Satpathy, S. & Martin, R. M. Origin of the Two-Dimensional Electron Gas
Carrier Density at the LaAlO₃ on SrTiO₃ Interface. *Phys Rev Lett* **101**, 256801 (2008).
- 48 Son, W. J., Cho, E., Lee, B., Lee, J. & Han, S. Density and spatial distribution of charge
carriers in the intrinsic n-type LaAlO₃-SrTiO₃ interface. *Phys Rev B* **79**, 245411 (2009).
- 49 Seo, S. S. A. *et al.* Multiple conducting carriers generated in LaAlO₃/SrTiO₃
heterostructures. *Appl Phys Lett* **95**, 082107 (2009).
- 50 Moetakef, P. *et al.* Electrostatic carrier doping of GdTiO₃/SrTiO₃ interfaces. *Appl Phys Lett*
99, 232116 (2011).
- 51 Pentcheva, R. & Pickett, W. E. Charge localization or itineracy at LaAlO₃/SrTiO₃ interfaces:
Hole polarons, oxygen vacancies, and mobile electrons. *Phys Rev B* **74**, 035112 (2006).
- 52 Sing, M. *et al.* Profiling the Interface Electron Gas of LaAlO₃/SrTiO₃ Heterostructures with
Hard X-Ray Photoelectron Spectroscopy. *Phys Rev Lett* **102**, 176805 (2009).
- 53 Blochl, P. E. Projector Augmented-Wave Method. *Phys Rev B* **50**, 17953-17979 (1994).
- 54 Kresse, G. & Furthmuller, J. Efficiency of ab-initio total energy calculations for metals and
semiconductors using a plane-wave basis set. *Comp Mater Sci* **6**, 15-50 (1996).
- 55 Yu, L. P., Ranjan, V., Lu, W., Bernholc, J. & Nardelli, M. B. Equivalence of dipole correction
and Coulomb cutoff techniques in supercell calculations. *Phys Rev B* **77**, 245102 (2008).
- 56 Persson, C., Zhao, Y. J., Lany, S. & Zunger, A. n-type doping of CuInSe₂ and CuGaSe₂. *Phys
Rev B* **72**, 035211 (2005).
- 57 Freysoldt, C. *et al.* First-principles calculations for point defects in solids. *Rev. Mod. Phys.*
86 (2014).